Welding in the World
https://doi.org/10.1007/s40194-024-01765-x

RESEARCH PAPER

Investigation of the effects of beam oscillations in electron beam–welded S1100M TMCP steel

Raghawendra P. S. Sisodia[1] · Marcell Gáspár[1] · Sumit Ghosh[2] · Erika Hodúlová[3]

Received: 25 September 2023 / Accepted: 28 March 2024

Abstract

The development of thermomechanically controlled processed (TMCP) high-strength steel (HSS) has significantly contributed to designing and developing the intricate structural components. It has broader applications in the cranes and lifting process industry (base frame, crane jibs, and crane columns), trailers, agricultural and forestry machinery, earth-moving equipment, etc. However, the development of new-grade steels with higher tensile strength led to higher requirements for welded joints, and the associated weldability issues have inspired detailed studies on electron beam welding (EBW) with different beam oscillations. Beam oscillation application with EBW processes improves the welding efficiency, weld quality, weld geometry, keyhole, etc., affecting the welded joints mechanical and microstructural properties. Thus, the present study investigates the impact and comparison of various beam oscillations on the microstructural and mechanical properties of EB-welded S1100M steel. The influence of welding parameters on the microstructure of welded joints was analyzed using a scanning electron microscope (SEM) and electron backscattered diffraction (EBSD). The analysis focused on evaluation of grain sizes, morphologies, distributions, and crystallographic orientations of different phase constituents in fusion zone (FZ) and heat-affected zone (HAZ). The mechanical properties were analyzed using hardness, tensile, and Charpy V-notch impact tests. The texture in the FZ is typically random, while the HAZ typically exhibits a strong rolling texture. In general, the cooling rate in EBW is very fast, possibly resulting in a fine-grained structure and reduced formation of coarse second-phase particles in the weld zone. The elliptical beam oscillation showed the highest hardness in HAZ 450 HV10. Elliptical beam oscillation slightly improves the welded joint's tensile strength, and the impact test showed mixed fracture behavior.

Keywords Electron beam welding · Beam oscillations · S1100M · TMCP steels · Microstructural characterization · Electron backscatter diffraction · Mechanical property

1 Introduction

The development of high-strength steels (HSSs) has significantly contributed to the diverse fields of application in many industries [1]. With growing global concern over climate change and environmental issues, the steel manufacturer focuses on sustainability through decarbonization and recycling. Furthermore, steel is 100% recyclable and one of the most reused materials in the world [2]. As a result of the concern mentioned above, the steelmaking industry is focusing on continuous cutting-edge research and development for steel production with outstanding mechanical properties like improved toughness and high strength with reduced weight. As a result, there is a growing demand for HSSs with lower thickness and mechanical properties [1]. The attractive features of high-strength steels are achieved through developing novel steel production routes, advancements in steel

Recommended for publication by Commission IV—Power Beam Processes

✉ Raghawendra P. S. Sisodia
raghawendra.sisodia@uni-miskolc.hu

[1] Institute of Materials Science and Technology, Faculty of Mechanical Engineering and Informatics, University of Miskolc, Miskolc-Egyetemváros, Borsod-Abaúj-Zemplén 3515, Hungary

[2] Materials and Mechanical Engineering, Centre for Advanced Steels Research, University of Oulu, 90014 Oulu, Finland

[3] Division of Microstructure of Surfaces and Interfaces, Institute of Materials and Machine Mechanics, Slovak Academy of Sciences, 84513 Bratislava, Slovakia

Published online: 26 April 2024

manufacturing technology, and, more importantly, appropriate alloying with microalloying elements. Some production routes are normalizing, quenching, and tempering (Q + T), thermomechanically controlled processing of steels, etc. [1]. Nowadays, these steels are available up to a yield strength level of 1300 MPa and are classified as ultra-high-strength structural steels (UHSSSs) [3–5]. Because of their lightweight and higher load carrying capacity, thermomechanically control processed (TMCP) steels are more widely used in a variety of broad applications such as offshore industries, earth-moving equipment, and extensive applications in the high-loaded elements of traveling cranes, special bridge structures, timber trailers [6], vehicle industries, ship building [7], oil industry [8–12], etc. "Hot rolled flat products made of high yield strength steels for cold forming— Part 2: Technical delivery conditions for thermomechanically rolled steels" under EN 10149–2 [13] specifies TMCP steels with yield strength up to 960 MPa. However, ultra-high-strength structural grades of TMCP steels are now available up to 1100 MPa. Due to the controlled rolling production methodology involved, these steels usually have high yield strengths and good toughness properties because of their fine-grained tempered martensitic (TM) and partially bainitic (B) microstructures [8]. TM-rolled steels require significantly less alloying elements, especially less carbon, than normalized steels (NS) or Q + T steels. This steel has high resistance to cold cracking, good formability, and low carbon content or equivalent (CEV) [14, 15]. Furthermore, these steels comprised more microalloying elements (Nb, Ti, V) and other alloying elements. These alloying elements form carbides and nitrides, which provide grain refinement and precipitation-hardening effects [16]. Ti–rich nitrides cause smaller grain sizes in the coarse-grained heat-affected zone (CGHAZ) due to their high thermal stability [17, 18]. In the case of TMCP steels, the reduced carbon content results in a softer and finer-grained microstructure in the heat-affected zone (HAZ) [19, 20]. Thus, it imparts good weldability with welding technique like electron beam welding (EBW). Kopas et al. [21] conducted a comparative study on the mechanical properties and microstructural characteristics of gas metal arc welding (GMAW) and EBW on TMCP steel (min. yield strength of 770 MPa grade). Their results showed that the EBW process resulted in better mechanical properties for the welded joint, primarily attributed to a narrower HAZ. Mazur et al. [22] underlined the important significance of selecting an appropriate welding process to achieve optimal mechanical properties in high-strength low-alloyed steels, emphasizing the need to minimize heat exposure, and softening in the HAZ. All the characteristics mentioned above of this steel make it more reliable and can be applied in welded structures [8].

The EBW process usually has several advantages over the conventional arc welding processes like narrow fusion zone (FZ) and HAZ, lower linear heat input, low distortion, higher welding speed, higher penetration depth in single pass weld, higher energy density, quality weld, and higher strength [23, 24]. In the EBW process, we frequently use static beams with ideal parameters for welding the various materials. However, beam oscillation has been commonly applied in the high-energy beam welding of various alloys. Beam oscillations caused a dynamic power distribution around the beam's stationary position, resulting in increased heat flow inside the keyhole and broader fusion and HAZ. It helps in improving the mixing and restricting the segregation in the weld pool [25, 26], and thus, it helps to enhance weld size, penetration depth, and, therefore, mechanical characteristics; the formation of homogenous structures, particularly in the case of dissimilar material–welded joints; and the avoidance of flaws such as porosity [27] and cold and hot cracks [28–30]. The other significant benefits of beam oscillation are a reduction in the undercutting at the weld root, lowering hardness in the FZ and HAZ, etc. [31]. Trushnikov et al. [32] investigated the dependence of the weld profile on the changing distribution of bombarding electrons in the keyhole produced by oscillations. They found that the shape of the weld pool changed significantly. Dinda et al. [33] found that beam oscillation resulted in welds with homogeneous microstructures and decreased hardness when welding plain carbon steel to Fe-7%Al alloy. Furthermore, welded joint yield strength and ultimate tensile strength were unaltered. Ol'shanskaya et al. [34] demonstrated that beam oscillation directly affects the growth of the primary and secondary structures of the weld metal as the shape of the welded joint changes. Tümer et al. [35] showed that during the impact test of an EB-welded joint, FZ did not provide a sufficient toughness value due to its higher hardness and untempered martensite microstructure.

As a result, in this paper, it is exciting to investigate the concept of beam oscillations by applying the EBW process to produce S1100M steel joints. Autogenous EBW joints were made with a normal EBW process or no oscillation, with circular and elliptical beam oscillation, and the test results were compared to analyze the effect of beam oscillation on the mechanical and microstructural properties of the welded joints. Several investigations on the influence of beam oscillation on the welded joint of various dissimilar materials and alloys have previously been presented; however, there needs to be more studies with ultra-high-strength structural steels.

2 Experimental procedures

2.1 Material

The base material (BM) used in the study was S1100M, thermomechanically rolled steel with a thickness of 15 mm.

Table 1 Chemical composition of base material

Steel	Chemical compositions of the investigated base material (wt.%)													
	C	Si	Mn	P	S	Cr	Cu	Ni	Mo	V	Ti	Nb	B	CEV
S1100M	0.13	0.32	1.62	0.009	0.0015	0.63	0.047	0.32	0.62	0.066	0.011	0.037	0.0014	0.68

Table 2 Mechanical properties of base material

Material	Mechanical properties of the investigated base material				
	$R_{p0.2}$, MPa	R_m, MPa	A_5, %	CVN_{-40} °C, J	HV10
S1100M	1100	1120–1300	8	27	383 ± 3*

*Measured in the laboratory

The plates with the dimension of 150 × 50 mm ($L \times W$) were cut, and the joining faces of the plates were machined precisely by the milling machine to the maximum allowable air gaps of 0.20 mm along the welded joint to be produced to secure precise fit for the welding. The base material's chemical composition (based on the manufacturer material certificate) and mechanical properties [36] are shown in Tables 1 and 2, respectively.

Based on the data in Table 1, the calculated carbon equivalent (CEV) for the S1100M steel according to standard EN 1011–2 [37] was 0.68.

2.2 Experiments

2.2.1 Electron beam welding (EBW)

The welding was performed by using the electron beam welding robotized device PZ EZ 30 STU complex (First Welding Company, Bratislava, Slovakia) equipped with two electron beam guns with a power of 30 kW for each gun, a vacuum chamber with dimensions of 1800 × 2360 × 3150 mm, and volume of 13.4 m^3 and the pumping system allowing reaching the vacuum of 5×10^{-2} Pa within 25 min, and the vacuum in an electron gun was 10^{-5} Pa. The vacuum pressure in the chamber was 9.8×10^{-5} Pa. Before welding, the samples were cleaned with acetone and dried. Prior to welding, the samples were demagnetized to prevent beam deflection. The samples were placed on a workbench in the vacuum chamber. Jigs were used to prevent deformation. The EBW trials were conducted to obtain the optimal parameters (Table 3) with the full penetration for the normal EBW, with circular and elliptical beam oscillation. Focusing current (I_f) of 920 mA and accelerating voltage of 55 kV were used. The working distance was 200 mm. A circular and elliptical oscillation pattern with a frequency of 500 Hz was applied. The oscillation pattern was set up using the M631 Arbitrary Waveform Generator, where the diameter of the oscillation circle was adjusted through peak-peak voltage (V_{pp}) of about 200 mV. In the case of elliptical oscillation, the dimension was set through peak-peak voltage (V_{pp}) of about 400 mV in length and 200 mV in width. Then, the experiments were done with different oscillations while the accelerating voltage (U_a) in kilovolt, beam current (I_b) in milliampere, and welding velocity (v) in millimeters per second were kept constant. The calculated welding linear heat input was 0.462 kJ/mm.

2.2.2 Microscopic test

The samples for light optical microscope (LOM), scanning electron microscope (SEM), and electron backscattering diffraction (EBSD) observations were sectioned transversely through the weld. For LOM and SEM microscopy, the sectioned samples were polished with different grades of SiC polishing papers, followed by diamond polishing [38]. The specimens were then etched for 10 s with 2% Nital. The metallographic observations were done using an Axio Observer D1m (Zeiss) inverted LOM for BM, HAZ, and FZ. A Zeiss Sigma FE-SEM with an EBSD detector was used for SEM and EBSD characterizations. Additional polishing with colloidal silica was conducted before the EBSD measurements. A step size of 0.05 µm was utilized.

Table 3 The EBW optimal parameters

Steel	Welding parameters						
	Oscillation type	Accelerating voltage (U_a), (kV)	Beam current (I_b) (mA)	Welding velocity (v) (mm/s)	Focussing current (I_f) (mA)	Frequency (Hz)	Channel voltage A-B (mV)
S1100M	Normal EBW	55	280	30	920		—
	Circular EBW	55	280	30	920	500	200–200
	Elliptical EBW	55	280	30	920	500	200–400

2.2.3 Hardness and tensile test evaluation

The hardness tests were conducted using a Reicherter UH250 universal macrohardness tester with a load of 10 kg and a 10-s dwell time in accordance with EN ISO 6507–1 [39]. For tensile tests, sub-size specimens according to the ASTM E8/E8M [40] were machined from the transverse (perpendicular to the welding direction) of the EB-welded butt joint. The tensile strength of all welded specimens was determined using a MTS 322 testing machine at room temperature. The samples were milled and etched to see the fracture along the welded specimens by viewing FZ and HAZ from the welded plates.

2.2.4 Impact toughness tests

The Charpy V-notch (CVN) pendulum impact tests were performed using Heckert equipment on sub-size specimens at − 40 °C in accordance with EN ISO 148–1 [41] standards to evaluate the impact energy of BM, HAZ, and FZ. Three Charpy V-Notch sub-size specimens with 10 × 5 × 55 mm dimensions were tested at − 40 °C for BM, HAZ, and FZ.

3 Results of the examinations

3.1 Microscopic characterisation

Figure 1a–c shows light optical, scanning electron, and electron back scattering diffraction (EBSD) micrographs of the as-received S1100M base material, respectively. Base material microstructure mainly consists of tempered martensite (TM) and martensite laths. Tempered martensite contains dispersed cementite precipitates embedded within laths.

The transverse cross section of the welded joint for the normal EBW, with circular beam oscillation and with elliptical beam oscillation, is shown in Fig. 2a–c, respectively. The fusion zone (FZ) and different heat-affected sub-zones are shown in Fig. 2c.

From Fig. 2a–c, we can see that the overall width of the welded joint surface area of normal EBW and elliptical oscillation is nearly the same, but in the case of the elliptical oscillation, the beam cross section is wider throughout the bottom of the joint due to the mixing and stirring of the molten material, while in a normal EBW joint, it is more like a taper. The circular oscillating joint is the narrowest of all three.

Figures 4, 5, and 6 show the SEM and EBSD micrographs of the FZ and different heat-affected sub-zones for the normal EBW, with circular beam oscillation and with elliptical beam oscillation. From Figs. 4a, 5a, and 6a, it can be seen that FZ of normal, with circular and with elliptical beam oscillation, processed EBW consisted of lath martensitic (M) microstructures. The microstructure of the FZ strongly depends on the heat input and the cooling rate during welding. In normal EBW without oscillation, the heat input is more uniform and concentrated at the weld interface, leading to a smaller heat-affected zone. Circular or elliptical oscillation methods involve the movement of the electron beam, which can spread the heat distribution over a wider area. This can cause more heating of the adjacent material, leading to a larger HAZ compared to the more localized heat input of normal EBW. Additionally, in normal EBW, the rapid heating and subsequent rapid cooling can result in a smaller HAZ due to the shorter duration of exposure to elevated temperatures compared to oscillation techniques, where the material may experience longer heat exposure and slower cooling rates. Thus, beam oscillation changes the heat input rate to the material and consequently affects the evolution of the microstructure. Existence of fine carbide precipitates together with negligible fraction of martensite/austenite (M/A) island is also revealed in Figs. 4a, 5a, and 6a. During EBW, the high heat input and subsequent rapid cooling can cause carbides to precipitate within the martensite

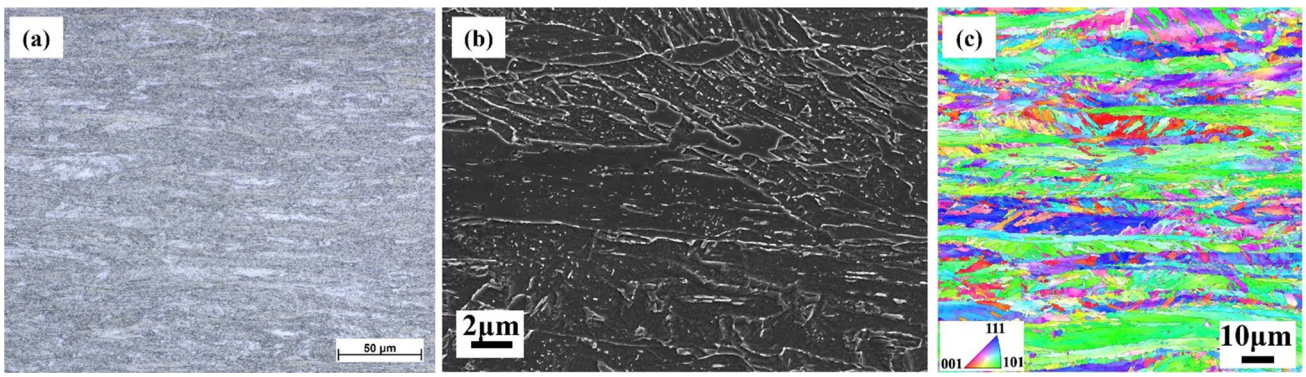

Fig. 1 Base material (S1100M) microstructure: **a** optical, **b** SEM, and **c** inverse pole figure (IPF) micrographs

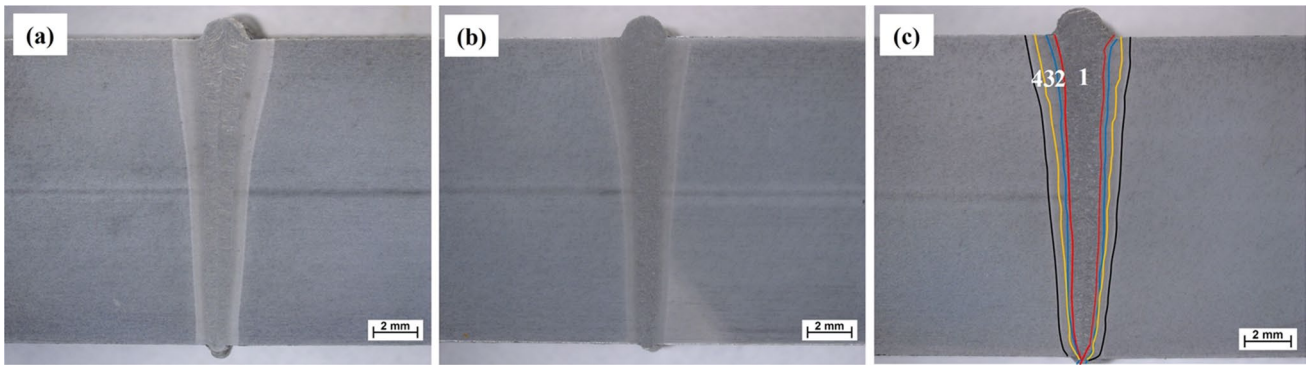

Fig. 2 Light optical micrographs of the weld cross section. **a** Normal EB. **b** Circular oscillation. **c** Elliptical oscillation. 1—fusion zone (FZ), 2—coarse-grained HAZ (CGHAZ), 3—fine grained HAZ (FGHAZ), 4—intercritical HAZ (ICHAZ)

laths. M-A constituents result from rapid heating and subsequent cooling with carbon enrichment during welding cycle [42]. The determination of M_s and M_f temperatures for the S1100M steel was determined using JMatPro® software as shown in Fig. 3.

Figures 4b, 5b, and 6b represent the inverse pole figure (IPF) maps of FZ for EBW specimens with normal, circular, and elliptical oscillation. It is observed that beam oscillation (both circular and elliptical) resulted in equiaxed grain within fusion zone, attributed to heat mixing and the evolution of random texture. Beam oscillation during electron beam welding promotes equiaxed grain formation within the fusion zone by enhancing heat mixing and disrupting the preferential growth of columnar grains, leading to a more uniform distribution of temperature and random grain orientation [43].

The HAZ can be divided into three sub-regions, such as coarse-grained HAZ (CGHAZ), fine-grained HAZ (FGHAZ), and intercritical HAZ (ICHAZ). In HAZ adjacent to FZ (i.e., CGHAZ zone), martensitic microstructure with average prior austenite grain (PAG) size of ~ 24 µm is observed in normal EBW specimen (Figs. 4d, 5d, and 6d), while circular and elliptical oscillation exhibits PAG of ~ 11 and 9 µm, respectively. Other than PAG grain size, no more morphological changes noticed between three welding conditions (Figs. 4c, 5c, and 6c).

In the ICHAZ zone, extremely fine martensitic microstructure with an average PAG size of ~ 6 µm is observed in normal EBW specimen (Figs. 4f, 5f, and 6f), while circular and elliptical oscillation exhibits a PAG of ~ 3.3 and 2.8 µm, respectively. In the FGHAZ zone, the average PAG grain size of all three conditions exhibits ~ 2 µm.

Fig. 3 Estimation of M_s and M_f temperature for S1100M steel

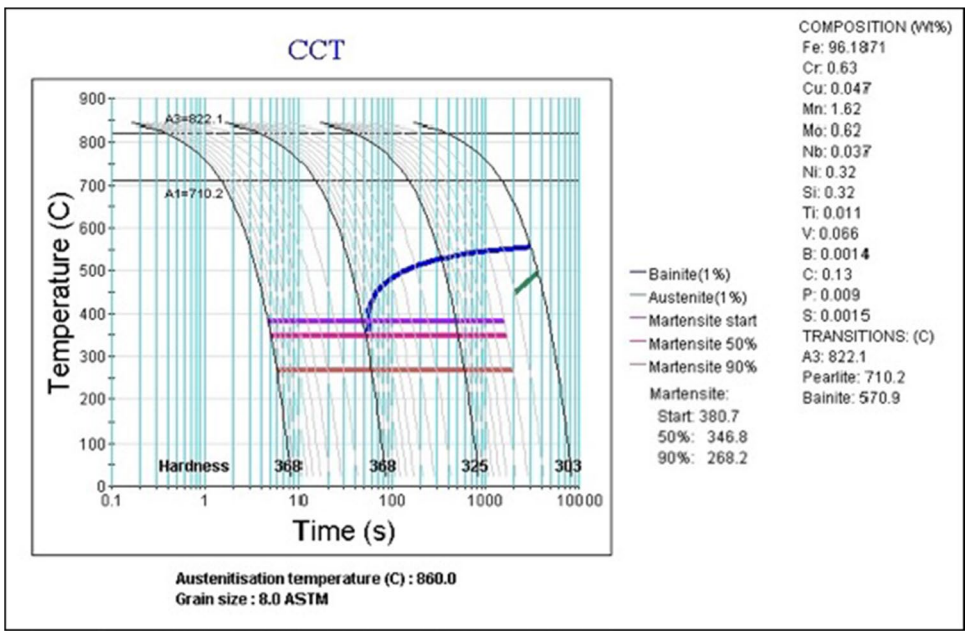

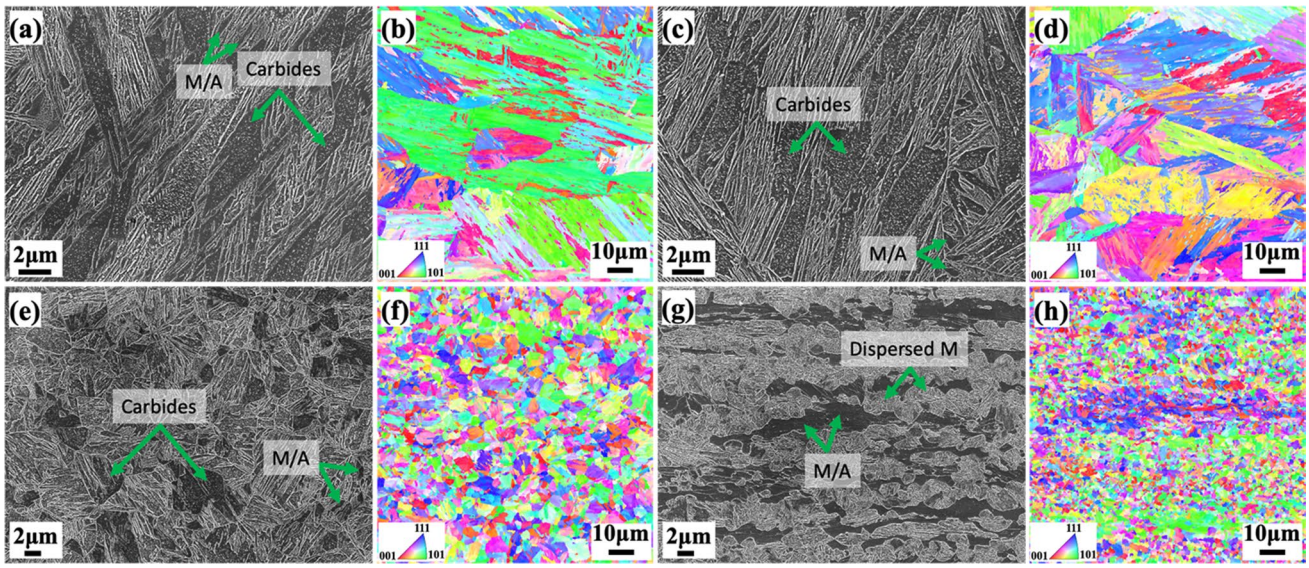

Fig. 4 S1100M SEM and EBSD IPF micrographs of normal EBW specimen without any oscillation: **a**, **b** FZ; **c**, **d** CGHAZ; **e**, **f** ICHAZ; and **g**, **h** FGHAZ, respectively

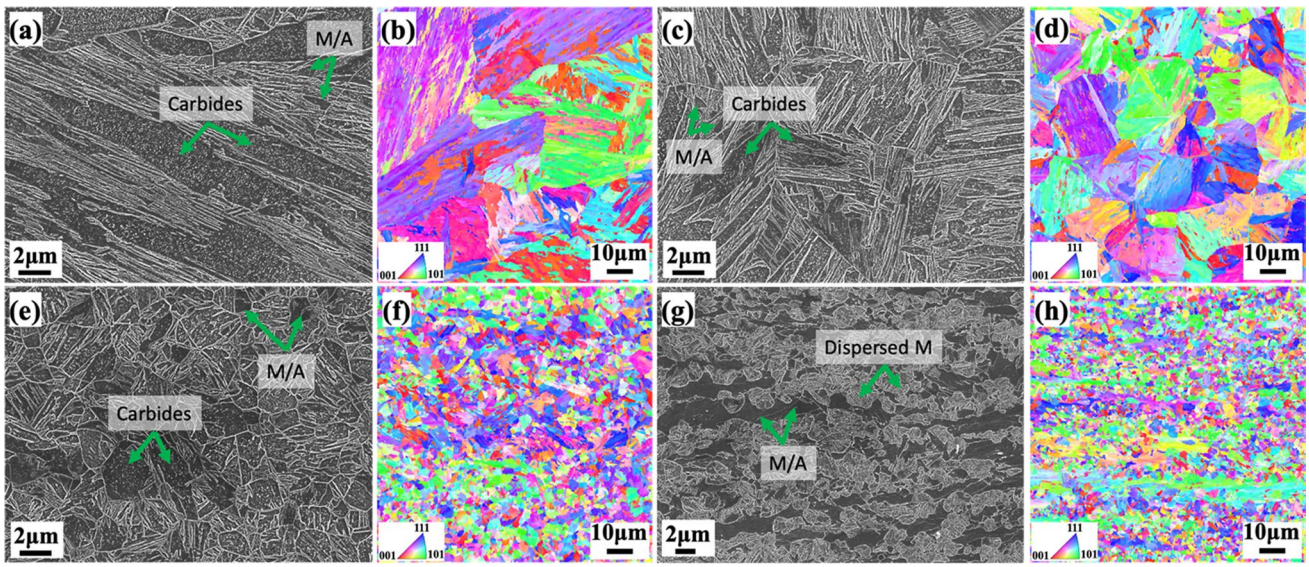

Fig. 5 S1100M SEM and EBSD IPF micrographs of EBW specimen with circular oscillation: **a**, **b** FZ; **c**, **d** CGHAZ; **e**, **f** ICHAZ; and **g**, **h** FGHAZ, respectively

Overall, microstructural observation of EBW specimens with and without oscillation conditions clearly showed a substantial variation of grain size across the welded joint for all the welded samples. Such heterogeneity in microstructure can be attributed to temperature gradients attained during EBW. Based on the observed variation of the grain size, the CGHAZ and ICHAZ of EBW with elliptical oscillation specimen microstructure exhibit finer PAG size. Thus, elliptical oscillation provides more control overheat distribution and promotes better mixing of molten metal compared to circular oscillation or normal EBW, leading to finer prior austenite grain boundaries. Furthermore, while beam oscillation can have a profound effect on the grain size distribution within the HAZ, its impact on the FZ is relatively minimal. The rapid solidification kinetics in the FZ tend to dominate over any additional refinement that oscillation might offer. Consequently, while there may be some minor variations or localized effects, overall, the grain size in the

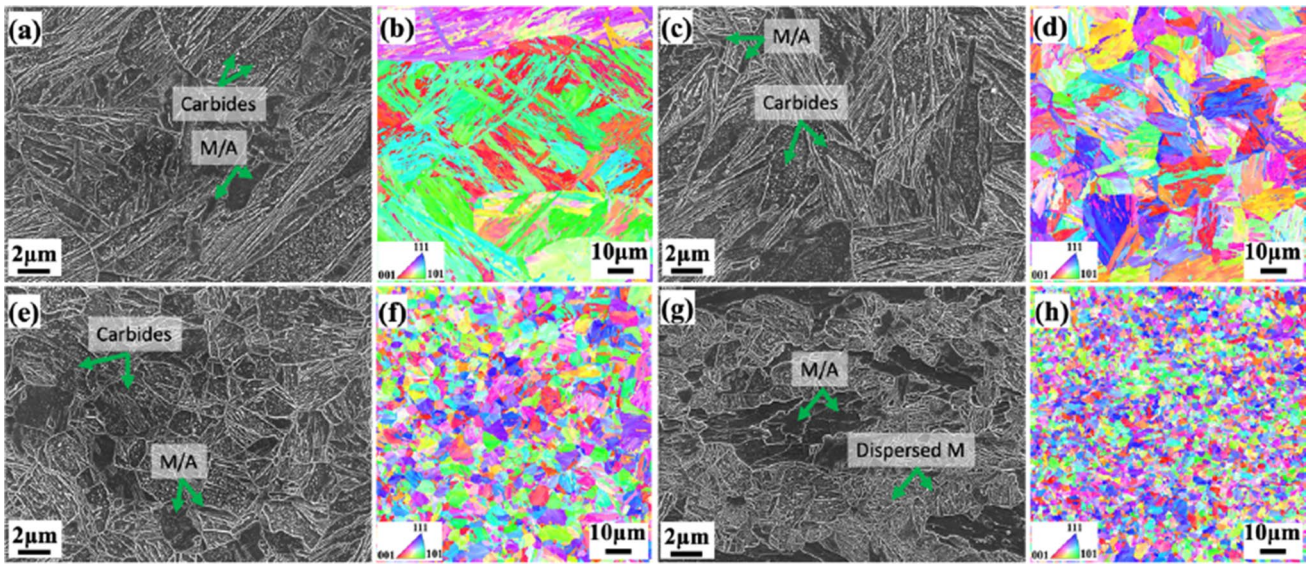

Fig. 6 S1100M SEM and EBSD IPF micrographs of EBW specimen with elliptical oscillation: **a**, **b** FZ; **c**, **d** CGHAZ; **e**, **f** ICHAZ; and **g**, **h** FGHAZ, respectively

FZ remains largely unaffected by the type of beam oscillation employed.

3.2 Macrohardness

The macrohardness value was measured over the welded joint transverse cross section below 0.2 mm from the top edge of a simple macro test specimen in the *y*-direction (transversal) and the spacing of 0.5 mm between the indentation points in the *x*-direction after surface preparation with grinding and polishing. Evaluation was performed according to the EN 15614–1 standard [44], which implied $HV_{max} = 450$ HV (HV10 or HV5) hardness for the welded joints (including HAZ) of quenched and tempered high-strength steels belonging to the third group of EN ISO/TR 15608 (quenched and tempered steel) [45] and $HV_{max} = 380$ HV10 for the thermomechanically treated steels belonging to the second group of EN ISO/TR 15608 (thermomechanically treated fine-grain steels) [45]. However, these criteria are not valid for this 1100 MPa grade because it is not considered in this classification system.

Figure 7 depicts the macroindentations of various locations (BM, HAZ, and FZ) along the specimens for the S1100M joints for normal EBW, circular beam, and elliptical beam oscillation.

The as-received base metal S1100M had a measured macrohardness of approximately 383 ± 3 HV10. The macrohardness at the center of the FZ for the normal EBW was 399 HV10, while that for circular beam oscillation was 403 HV10, which has a nearly similar macrohardness. However, the hardness of FZ for the elliptical oscillation was 410 HV10. The

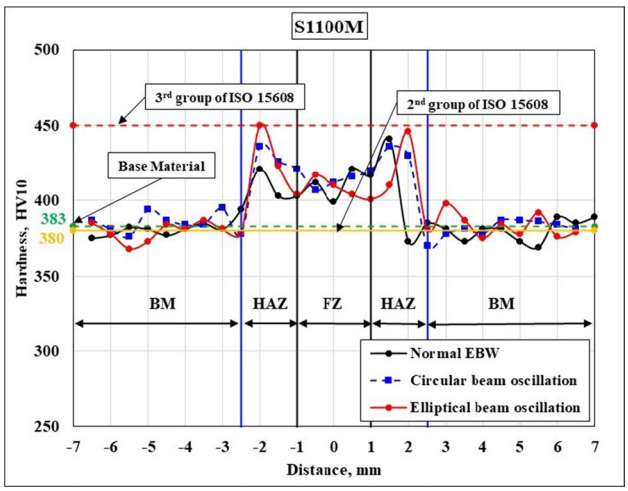

Fig. 7 S1100M, macrohardness; normal EBW, circular, and elliptical beam oscillation

elliptical beam oscillation showed the highest macrohardness in HAZ 450 HV10, normal EBW showed 441 HV10, and circular oscillation measured 436 HV10. The average measured hardness for FZ in the elliptical oscillation (407 HV10) case was nearly similar to normal EBW (410 HV10) and circular oscillation (412 HV10), but for HAZ in the case of elliptical oscillation joint (437 HV10) was higher than both normal EBW (406 HV10) and circular oscillation (428 HV10). The use of circular beam oscillation in the EBW of S1100M steel joints caused a nearly similar average hardness in FZ and a slightly higher HAZ than normal EBW. However, elliptical oscillation yielded the highest average HAZ hardness among

the three processes (normal EBW, circular oscillation, and elliptical oscillation). The highest hardness in CGHAZ during elliptical oscillation, as well as the overall average HAZ hardness, can be attributed to the finer grain size achieved through elliptical oscillation, which facilitates more precise control overheat distribution and, in turn, promotes better mixing of molten metal, leading to finer prior austenite grain boundaries compared to circular oscillation or normal EBW process. It is evident from the measured results that in all three cases of the EB-welding process, the average hardness of FZ and HAZ exceeded that of the BM. This increase in hardness can be correlated to the formation of fresh martensite microstructure in FZ and refined PAG size within HAZ.

3.3 Tensile properties

Tensile test results for EB-welded joints with different beam oscillations are shown in Table 4.

According to the material data sheet [36], the tensile strength of the BM was given in the range of 1120–1300 MPa. From our test results, it can be clearly seen that in all three cases of welded joints (normal EBW, circular, and elliptical beam oscillated joints), the strength values pass the minimum threshold of the given range provided in the material data sheet. The average tensile strength is nearly similar in the case of normal EBW and with circular beam oscillation joints. However, a considerable increase in tensile strength (2.5%) of elliptical oscillation welded joints was observed compared to the normal EBW and circular oscillation joint, which can be marked in Table 4. This slight rise in the tensile strength may be due to the higher average hardness of HAZ in the elliptical oscillated welded joint and also due to the refinement of the microstructures in the FZ and HAZ, as shown in Figs. 5 and 6. Also, it is crucial to remark that the elliptical welded joint's tensile strength reached the maximum range of strength level provided. The fracture location of joints for all three methods is shown in Fig. 8.

In all three cases of welding conditions, fracture in tested specimens took place in the base material section of the tensile test specimens, which can be seen in Fig. 8. From Fig. 2c, it is evident that the overall width of the welded joint covers a larger surface during the elliptical oscillation of the beam compared to the normal and circular oscillation, which also results in more profound fusion at the joint surface. This helped to increase interfacial bonding and enhanced strength in the elliptical oscillated EB-welded joint. However, we can also observe from the microstructural analysis results that the variations of the grain size, the CGHAZ, and the ICHAZ of EBW with elliptical oscillation specimen microstructure exhibit a finer PAG size. Thus, all the factors mentioned above together contribute to increased tensile strength.

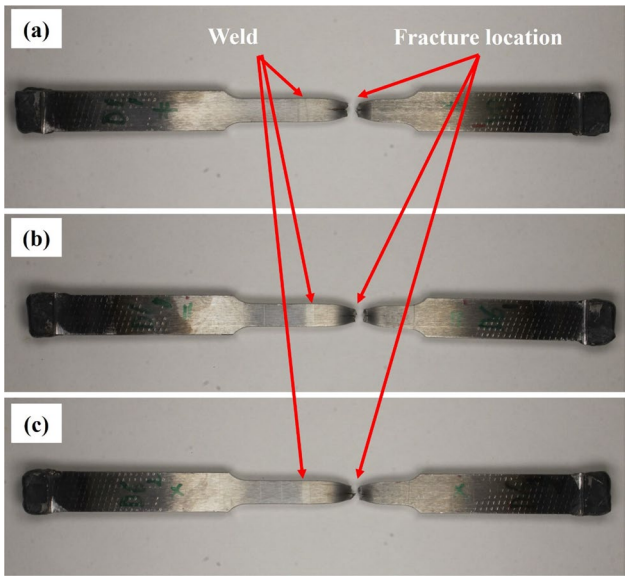

Fig. 8 Tensile fracture location. **a** Normal EBW, **b** circular beam location, and **c** elliptical beam oscillation joints (camera photo)

3.4 Charpy V-notch impact test

The Charpy V-notch impact test was used to quantify the toughness of the welded joints at the base material's guaranteed operating temperature [33]. According to the material data sheet [36], the required minimum impact energy (CVN) (transverse direction test) for S1100M steel was 27 J at − 40

Table 4 Tensile properties of EB-welded joints

Steel	Tensile results of EB-welded joints				
	Process	Sample No	Tensile strength (MPa)	Average tensile strength (MPa)	Fracture location
S1100M	Normal EBW	1	1164	1164	Base material
		2	1164		Base material
	Circular	1	1165	1165	Base material
		2	1164		Base material
	Elliptical	1	1191	1192	Base material
		2	1192		Base material

°C. The notches in the Charpy specimens were incised using the wire EDM cutting process with 3 mm diameter wire in FZ and HAZ. The macroscopic fracture surfaces of the selected Charpy V-notch test specimens tested at − 40 °C are presented in Fig. 9.

The fracture surfaces of the selected specimen from the BM, HAZ, and FZ performed at − 40 °C under various welding conditions like normal EBW, circular, and elliptical beam oscillation were examined using SEM. The results are shown in Fig. 10a–g. Ductile fracture surfaces are characterized primarily by the presence of dimples and microvoids, whereas brittle surfaces typically exhibit cleavage facets, river patterns, and a transcrystalline nature [9, 46]. The BM fractured surfaces (Fig. 10a) show a ductile fracture pattern characterized by the presence of dimple morphology across various locations of the fractured surface. The HAZ tested fractured surface of normal EBW (Fig. 10b) exhibits a ductile pattern featuring typical small dimples and microvoids. However, in the case of circular and elliptical oscillation (Fig. 10c, d), the fracture surfaces predominantly present the brittle behavior characterized by cleavage fractures with a river pattern (Fig. 10d).

In the case of the FZ, the fractured surface resulting from normal EBW and circular beam oscillation (Fig. 10e, f) predominantly shows brittle characteristics. However, for the elliptical beam oscillation, the fractures exhibit a mixed type, characterized by presence of both cleavage fractures and dimples (Fig. 10g).

The comparison of the CVN values for the normal EBW joints, circular beam, and elliptical beam oscillated joint from the investigated S1100M material are presented in Table 5, along with the average (Avg.) CVN, corrected CVN, and toughness (J/cm^2). To compare Charpy test results with normal size specimens, a correction needs to apply to account for the reduced thickness. There are several articles in which sub-size Charpy specimens were investigated, and the correction method was adopted for the reduced-size Charpy specimens. Schneider et al. [47] analyzed the toughness of S960MC structural steel with a thickness of 8 mm. In the study, they used sub-size

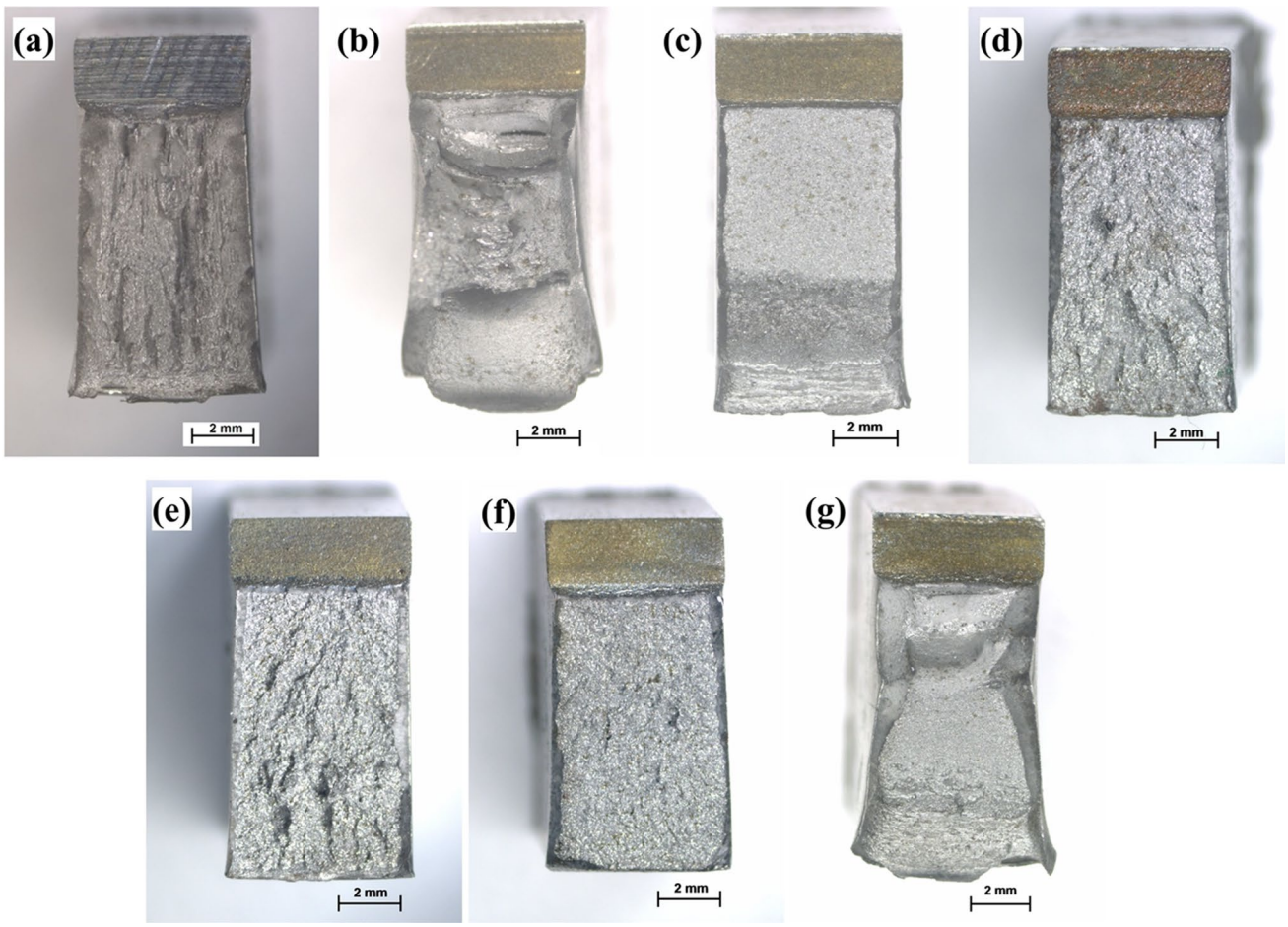

Fig. 9 Selected specimen macrofractured surfaces at − 40 °C: BM **a** S1100M steel; HAZ **b** normal EBW, **c** circular beam, and **d** elliptical beam oscillation joints; FZ **e** normal EBW, **f** circular beam, and **g** elliptical beam oscillation joints (macrophoto)

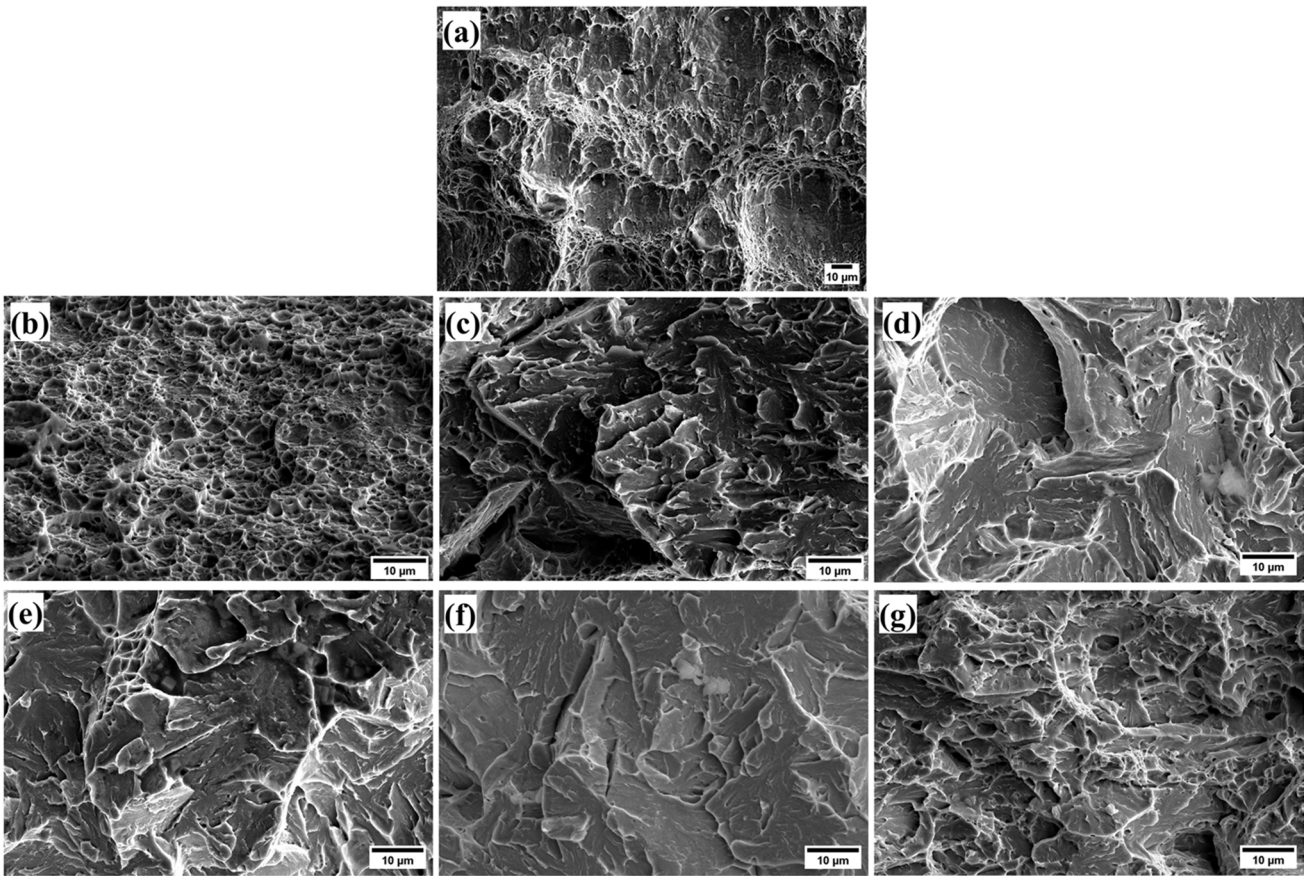

Fig. 10 Fractured surfaces for the selected specimens after Charpy impact testing at − 40 °C, BM **a** S1100M steel; HAZ **b** normal EBW, **c** circular beam, and **d** elliptical beam oscillation joints; FZ **e** normal EBW, **f** circular beam, and **g** elliptical beam oscillation joints

Table 5 Measured CVN values of EB-welded S1100M joints at − 40 °C

Oscillation types	Zone	Measured Charpy V-notch impact test values of EB-welded S1100M joints			
		Avg., J	Corr. Avg., J	Avg. toughness (Corr), J/cm^2	Remark
Base material	-	28	55	137	Ductile
Normal EBW	HAZ	39	78	195	Ductile
	FZ	10	20	52	Brittle
Circular oscillation	HAZ	12	24	58	Brittle
	FZ	11	22	53	Brittle
Elliptical oscillation	HAZ	9	18	45	Brittle
	FZ	23	46	109	Mixed

specimens with a dimension of $10 \times b \times 5$ mm, where b is the reduced width of the specimens. So, the correction of the reduced-size Charpy specimen test results can be obtained using the methods in which the test results are multiplied by a factor of 10/b. Guo et al. [48] in their study related to the laser beam welding of S960 high-strength steel used the same correction method for the reduced sub-size Charpy test specimens.

Accordingly, we have followed a similar approach in applying corrections to the energies we measured on 5-mm-thick specimens, i.e., by multiplying the absorbed energies by a factor of 2 (i.e., 10/5), and the corrected CVN and corrected CVN_{avg} and corrected toughness values are presented in Table 5.

The average impact energy of the three sub-size specimens of the investigated base material steel plates was 28

J, and the corrected CVN value was 55 J during the impact test.

The average corrected Charpy V impact energy for HAZ of the normal EBW joint is 78 J, which shows that it produced a significant increase in the average toughness value in HAZ, which was around 3.3 times higher compared to circular oscillated EB-welded HAZ toughness value (24 J) and 4.3 times higher than elliptical oscillated EB-welded HAZ toughness (18 J). The average hardness of the HAZ for the normal EBW process was the lowest (406 HV10) among the three different methods used: normal, circular, and elliptical oscillated beam oscillations, indicating the maximum toughness in the HAZ of the normal EBW joints. However, several other factors, like favorable grain boundary orientation and finer precipitate dispersion, may have contributed to the higher toughness in the HAZ of the normal EB-joint. Also, the EB weld has a very narrow HAZ, and it is sometimes tough to make the notch always into the same part of the HAZ.

The average corrected CVN values for FZ were observed to be highest in the case of an elliptical oscillated joint (46 J), which was 2.3 times higher than a normal EB-welded joint and two times higher than a circular beam oscillated joint. With the help of the elliptical beam oscillation's dynamic heating and cooling pattern, the fusion zone's thermal gradient can be minimized, and thus, the weld joint toughness is maintained.

4 Summary and conclusions

The following conclusions can be drawn from our investigations:

- The EBW of S1100M steel was successfully performed in normal EBW with circular and elliptical oscillations, and the mechanical and microstructural results were compared.
- The FZ of the normal EBW process, with circular and elliptical beam oscillation process EBW, consisted of lath martensitic (M) microstructures.
- SEM investigation of the FZ of all three EBW processes revealed the presence of fine carbide precipitates and a small fraction of martensite/austenite (M/A) island.
- From the inverse pole figure (IPF) maps of FZ for EBW specimens with normal, circular, and elliptical oscillation, it was observed that beam oscillation (both circular and elliptical) resulted in equiaxed grain within the fusion zone, attributed to heat mixing and the evolution of random texture.
- In HAZ adjacent to FZ (i.e., CGHAZ zone), martensitic microstructure with average prior austenite grain (PAG) size of ~ 24 μm is observed in normal EBW specimen (Figs. 4d, 5d, and 6d). At the same time, circular and elliptical oscillation exhibits PAG of ~ 11 and 9 μm, respectively. Besides PAG grain size, no more morphological changes were noticed between the three welding conditions.
- Based on the observed grain size variation, the CGHAZ and ICHAZ of EBW with elliptical oscillation specimen microstructure exhibit finer PAG size.
- Overall, the microstructural observation of EBW specimens with and without oscillation conditions showed a substantial grain size variation across the weld joint for all the welded samples.
- The as-received base metal S1100M had a measured macrohardness of approximately 383 ± 3 HV10.
- The average measured hardness for FZ in the elliptical oscillation (407 HV10) case was nearly similar to normal EBW (410 HV10) and circular oscillation (412 HV10).
- In the case of HAZ for the elliptical oscillation joint, the average hardness (437 HV10) was higher than both normal EBW (406 HV10) and circular oscillation (428 HV10).
- The FZ incised specimen of Charpy V-notch impact tests for the elliptical oscillated joint demonstrates a significant increase in toughness value, which is approximately 2.3 times and two times higher than the normal EB-welded and circular beam oscillated joint toughness value, respectively.
- The Charpy V-notch impact tests for HAZ of the normal EBW joint are 78 J, the highest among all the three cases.
- Fractographic analysis indicates that the BM and normal HAZ exhibit ductile characteristics, while the circular and elliptical HAZ display brittle behavior. Furthermore, the FZ demonstrates varying responses, with normal EBW and circular oscillation inducing brittle fractures, while elliptical oscillation results in a mixed fracture pattern.

Furthermore, the EBW with beam oscillation specially with elliptical beam oscillation study demonstrated positive application feasibility for high-strength structural steel; however, further research with different parameters, patterns, and techniques is required to analyze its more exclusive benefits in terms of improved mechanical properties.

Acknowledgements The authors wish to express their deep appreciation to Slovak University of Technology, Faculty of Materials Science and Technology researchers, Assoc. Prof. Pavel Kovacocy and MSc. Marian Pavlik, for their generous cooperation in the production of the electron-welded joints used in this research. The authors are grateful to the Prof. Dr. Valéria Mertinger, Kovács Árpád Győző, and Dr. Koncz-Horváth Dániel, Institute of Physical Metallurgy, Metal Forming and Nanotechnology at the University of Miskolc, for the scanning electron microscope for the fractography analysis.

Author contribution Raghawendra P. S. Sisodia: conceptualization, methodology, investigation, data curation, formal analysis, writing

original draft, writing, review, and editing. Marcell Gáspár: writing, review, and editing. Sumit Ghosh: microstructural investigation, formal analysis, data curation, writing, review, and editing. Erika Hodúlová: resources, writing, review, and editing.

Funding Open access funding provided by University of Miskolc. This paper and participation in the 76th IIW (2023) annual assembly and international conference on welding and joining, Singapore, were supported by a grant funded by the Institute of Materials Science and Technology, Faculty of Mechanical Engineering and Informatics, University of Miskolc, Miskolc-Egyetemvaros, 3515 Hungary. The participation in the IIW2023 conference was also supported by the Hungarian Welding Society (MAHEG), the MHtE Alapítvány (MHtE Foundation) and the Flexman Robotics Ltd. SG like to thank Jane ja Aatos Erkon säätiö (JAES) and Tiina ja Antti Herlinin säätiö (TAHS) foundation for their financial support to perform advanced microstructural (SEM and EBSD) characterization with the support of the Centre for Materials Analysis, University of Oulu, Finland.

Data availability The data supporting the results of this article are included within the article.

Declarations

Competing interests The authors declare no competing interests.

References

1. Sisodia RPS (2021) High energy beam welding of advanced high strength steels, PhD Thesis. University of Miskolc
2. Juan Enrique VA (2023) Sustainability assessment in the steel industry using partial least squares - structural equation model. World Dev Sustain 2:100054. https://doi.org/10.1016/j.wds.2023.100054
3. Tomków J, Landowski M, Fydrych D, Rogalski G (2022) Underwater wet welding of S1300 ultra-high strength steel. Mar Struct 81:. https://doi.org/10.1016/j.marstruc.2021.103120
4. Tümer M, Schneider-Bröskamp C, Enzinger N (2022) Fusion welding of ultra-high strength structural steels – a review. J Manuf Process 82:203–229. https://doi.org/10.1016/j.jmapro.2022.07.049
5. Gáspár M, Sisodia RPS (2017) Weldability analysis of Q + T and TMCP high strength steels by physical simulation. In: the IIW 2017 International Conference: Green Welding Technologies for Effective and Reliable Manufacturing. Shanghai, China
6. Gsodam reduced timber trailer weight by 20% with Strenx® steel. https://www.ssab.com/en/news/2023/05/gsodam. Accessed 16 Jun 2023
7. Górka J (2015) Weldability of thermomechanically treated steels having a high yield point. Arch Metall Mater 60:469–475. https://doi.org/10.1515/amm-2015-0076
8. Górka J, Janicki D, Fidali M, Jamrozik W (2017) Thermographic assessment of the HAZ properties and structure of thermomechanically treated steel. Int J Thermophys 38:1–21. https://doi.org/10.1007/s10765-017-2320-9
9. Sisodia RPS, Gáspár M (2021) Experimental assessment of microstructure and mechanical properties of electron beam welded S960M high strength structural steel. Manuf Lett 29:108–112. https://doi.org/10.1016/j.mfglet.2021.05.004
10. Sisodia R, Gáspár M (2023) Dataset on instrumented Charpy V-notch impact tests of different zones of electron beam welded S960M steel. Data Br 47:108949. https://doi.org/10.1016/j.dib.2023.108949
11. Lisiecki A (2014) Welding of thermomechanically rolled fine-grain steel by different types of lasers. Arch Metall Mater 59:1625–1631. https://doi.org/10.2478/amm-2014-0276
12. Kovács J, Lukács J (2023) Influence of filler metals on microstructure and mechanical properties of gas metal arc welded high strength steel. In: Jármai K, Cservenák Á (eds) In: Jármai, K., Cservenák, Á. (eds) Vehicle and automotive engineering 4. VAE 2022. Lecture notes in mechanical engineering. Springer International Publishing, Cham, pp 995–1005
13. EN 10149–2, Hot rolled flat products made of high yield strength steels for cold forming— part 2: technical delivery conditions for thermomechanically rolled steels
14. Koncsik Z, Lukács J, Nagy G (2022) Fracture mechanical analysis of Gleeble simulated heat affected zones in high strength steels. Period Polytech Mech Eng 66:83–89. https://doi.org/10.3311/PPME.19077
15. Schaupp T, Schröepfer D, Kromm A, Kannengiesser T (2014) Welding residual stress distribution of quenched and tempered and thermo-mechanically hot rolled high strength steels. Adv Mater Res 996:457–462. https://doi.org/10.4028/www.scientific.net/AMR.996.457
16. Gorka J, Poloczek T, Kotarska A, Jamrozik W (2021) Analysis of precipitates in heat treated thermo- mechanically processed steel with a high yield strength. IOP Conf Ser Mater Sci Eng. https://doi.org/10.1088/1757-899X/1182/1/012026
17. Kenneth Easterling (1992) Introduction to the physical metallurgy of welding., 2nd ed.
18. Zhang L, Kannengiesser T (2014) Austenite grain growth and microstructure control in simulated heat affected zones of microalloyed HSLA steel. Mater Sci Eng A 613:326–335. https://doi.org/10.1016/j.msea.2014.06.106
19. Schaupp T, Schroepfer D, Kromm A, Kannengiesser T (2017) Welding residual stresses in 960 MPa grade QT and TMCP high-strength steels. J Manuf Process 27:226–232. https://doi.org/10.1016/j.jmapro.2017.05.006
20. Yue X, Lippold J, Alexandrov B, Babu S (2012) Continuous cooling transformation behavior in the CGHAZ of naval steels. Weld J 91:67S-75S
21. Kopas P, Sága M, Jambor M et al (2018) Comparison of the mechanical properties and microstructural evolution in the HAZ of HSLA DOMEX 700MC welded by gas metal arc welding and electron beam welding. MATEC Web Conf 244. https://doi.org/10.1051/matecconf/201824401009
22. Mazur M, Ulewicz R, Novy F, Szataniak P (2013) The structure and mechanical properties of domex 700 MC steel. Commun - Sci Lett Univ Žilina 15:54–57. https://doi.org/10.26552/com.c.2013.4.54-57
23. Schultz H (1993) Electron beam welding. Abington Publishing, Cambridge

24. Węglowski MS, Błacha S, Phillips A (2016) Electron beam welding - techniques and trends - review. Vacuum 130:72–92. https://doi.org/10.1016/j.vacuum.2016.05.004
25. Babu NK, Raman SGS, Murthy CVS, Reddy GM (2007) Effect of beam oscillation on fatigue life of Ti-6Al-4V electron beam weldments. Mater Sci Eng A 471:113–119. https://doi.org/10.1016/j.msea.2007.03.040
26. Kar J, Roy SK, Roy GG (2016) Effect of beam oscillation on electron beam welding of copper with AISI-304 stainless steel. J Mater Process Technol 233:174–185. https://doi.org/10.1016/j.jmatprotec.2016.03.001
27. Kar J, Dinda SK, Roy GG et al (2018) X-ray tomography study on porosity in electron beam welded dissimilar copper–304SS joints. Vacuum 149:200–206. https://doi.org/10.1016/j.vacuum.2017.12.038
28. Sisodia RPS, Gáspár M, Hodúlová E (2023) Effect of beam oscillation and focusing on the electron beam welded 1100M high strength structural steel joint. J Phys ConfSer 2443. https://doi.org/10.1088/1742-6596/2443/1/012008
29. Tao J, Wu J, Liu Z et al (2022) Influence of different beam oscillation patterns in electron beam welding of niobium sheets with different thickness. Materials (Basel) 15:1–14. https://doi.org/10.3390/ma15113778
30. Koleva E, Koleva L, Trushnikov D et al (2022) Multicriterial optimization strategies for electron beam welding processes. J Phys Conf Ser 2240:012038. https://doi.org/10.1088/1742-6596/2240/1/012038
31. Komerla K, Gach S, Vossel T et al (2019) The effect of beam oscillations on the microstructure and mechanical properties of electron beam welded steel joints. Int J Adv Manuf Technol 102:2919–2931. https://doi.org/10.1007/s00170-019-03355-4
32. Trushnikov DN, Koleva EG, Mladenov GM, Belenkiy VY (2013) Effect of beam deflection oscillations on the weld geometry. J Mater Process Technol 213:1623–1634. https://doi.org/10.1016/j.jmatprotec.2013.03.028
33. Dinda SK, Basiruddin Sk M, Roy GG, Srirangam P (2016) Microstructure and mechanical properties of electron beam welded dissimilar steel to Fe–Al alloy joints. Mater Sci Eng A 677:182–192. https://doi.org/10.1016/j.msea.2016.09.050
34. Ol'shanskaya TV, Trushnikov DN, Belen'kii VY, Mladenov GM (2013) Effect of electron beam oscillations on the formation of the structure and properties of the welded joint. Weld Int 27:881–885. https://doi.org/10.1080/09507116.2013.796638
35. Tümer M, Pixner F, Enzinger N (2022) Residual stresses, microstructure, and mechanical properties of electron beam welded thick S1100 steel. J Mater Eng Perform 31:2136–2146. https://doi.org/10.1007/s11665-021-06348-1
36. Data-sheet-alform-x-treme-voestalpine. https://www.voestalpine.com/alform/en/Products/x-treme. Accessed 18 Jun 2023
37. EN 1011–2, Welding - recommendations for welding of metallic materials - part 2: arc welding of ferritic steels
38. Sisodia RPS, Gáspár M, Sepsi M, Mertinger V (2021) Dataset on full width at half maximum of residual stress measurement of electron beam welded high strength structural steels (S960QL and S960M) by X-ray diffraction method. Data Br 38:107341. https://doi.org/10.1016/j.dib.2021.107341
39. EN-ISO 6507–1 Metallic materials - Vickers hardness test - part 1: test method
40. ASTM E8/E8M, Standard test methods for tension testing of metallic materials
41. EN ISO 148–1, Metallic materials, Charpy pendulum impact test, Part 1: Test method
42. Li X, Shang C, Ma X et al (2017) Elemental distribution in the martensite–austenite constituent in intercritically reheated coarse-grained heat-affected zone of a high-strength pipeline steel. Scr Mater 139:67–70. https://doi.org/10.1016/j.scriptamat.2017.06.017
43. Singh V, Srirangam P, Roy GG (2023) Effect of beam oscillation on microstructure and mechanical properties of electron beam welded EN25 steel. Materials (Basel) 16.https://doi.org/10.3390/ma16072717
44. EN 15614–1, Specification and qualification of welding procedures for metallic materials — welding procedure test — part 1: arc and gas welding of steels and arc welding of nickel and nickel alloys
45. EN ISO/TR 15608 Welding- guidelines for a metallic materials grouping system
46. Sisodia RPS, Gáspár M (2022) An approach to assessing S960QL steel welded joints using EBW and GMAW. Metals (Basel) 12.https://doi.org/10.3390/met12040678
47. Schneider C, Ernst W, Schnitzer R et al (2018) Welding of S960MC with undermatching filler material. Weld World 62:801–809. https://doi.org/10.1007/s40194-018-0570-1
48. Guo W, Crowther D, Francis JA et al (2015) Microstructure and mechanical properties of laser welded S960 high strength steel. JMADE 85:534–548. https://doi.org/10.1016/j.matdes.2015.07.037